PLANETARY WAVES IN AN ASSIMILATION OF THREE MARS YEARS OF THERMAL EMISSION SPECTROMETER DATA FROM MARS GLOBAL SURVEYOR. S. R. Lewis[1], L. Montabone[1], P. L. Read[2], P. Rogberg[2], R. J. Wilson[3] and M. D. Smith[4], [1]Department of Physics & Astronomy, The Open University, Walton Hall, Milton Keynes MK7 6AA, UK (S.R.Lewis@open.ac.uk), [2]Atmospheric, Oceanic & Planetary Physics, Department of Physics, University of Oxford, Clarendon Laboratory, Parks Road, Oxford OX1 3PU, UK, [3]Geophysical Fluid Dynamics Laboratory, National Oceanic and Atmospheric Administration, Princeton, New Jersey, USA, [4]NASA Goddard Space Flight Center, Greenbelt, Maryland, USA.

Introduction: We investigate the dynamics of large-scale traveling and stationary planetary waves diagnosed from an analysis of profiles retrieved from the Thermal Emission Spectrometer (TES) [1] aboard the Mars Global Surveyor (MGS) spacecraft during its scientific mapping phase. The analysis was conducted by assimilating the TES temperature profile and total dust opacity retrievals [2] into a pseudo-spectral Mars general circulation model to produce a full, physically self-consistent record of all atmospheric variables stored at an interval of two hours over the entire MGS mapping phase. The data cover a period of about three Mars years, corresponding to the interval 1999–2004 on Earth. These include the year which contained the 2001 global dust storm [3] and two years of more moderate dust activity, although large regional storms occurred during southern hemisphere summer in both years and there was considerable atmospheric variability between all three years [4].

In the present paper we focus on the planetary wave activity, both traveling and stationary large-scale waves, in the assimilated record. Data assimilation is a particularly useful technique for the analysis of transient wave behaviour since it is capable of producing global, time-dependent atmospheric fields, which the assimilation scheme endeavours to make as consistent as possible with whatever observations are available. These atmospheric variables may be sampled from the model as often as desired, on a regular grid of points. If particular variables, or regions of the atmosphere, are not observed directly, the model will at least ensure that they are consistent with the laws of physics incorporated within it.

A complex climatology of transient waves is revealed, modulated by the large-scale topography and surface thermal properties, the time of year and, crucially, the amount of dust suspended in the atmosphere. Some individual case studies show the temporal and spatial structures of the waves in the assimilation record, although the large data set has by no means been fully explored. Companion papers discuss the thermal atmospheric tides [5] and the processes associated with the initiation of dust storms [6] from the same assimilated analysis.

Data Assimilation: The data have been analysed by assimilation into a pseudo-spectral Mars general circulation model [7], making use of a sequential procedure known as the analysis correction scheme [8], a form of the successive corrections method which has proved simple and robust in trial studies with artificial data under Martian conditions [9, 10]. The entire period has been assimilated, with varying model parameters, at a default model triangular spectral truncation at a total wavenumber 31 (T31), with non-linear products evaluated on a 96×48 dynamical horizontal grid (physical processes are evaluated on a reduced 72×36 grid) and using a stretched vertical grid on 25 sigma surfaces up to about 100 km altitude. Limited periods have been re-analysed with a high horizontal resolution model, truncated at total wavenumber 170 (T170), with a 512×256 dynamical grid and 384×196 physical process grid, in order to test sensitivity to model resolution.

Assimilation of the TES data using this technique during the MGS aerobraking hiatus has been described [11], as has an analysis of the thermal tidal behaviour throughout the MGS mapping phase [12]. The mapping phase assimilation has been validated by a cross-comparison of model temperature profiles sampled at the same time and place as profiles obtained by radio occultation, also using the MGS spacecraft [13]. The results of this assimilation procedure are further validated in this paper by comparing the planetary waves in the assimilation with those from direct synoptic mapping analyses of the TES retrievals.

The full period for which assimilated data is available is illustrated by Fig. 1, which shows the assimilated dust optical depth in the visible, averaged over all longitudes and converted to an equivalent optical depth at a standard reference pressure of 610 Pa. The Mars Years (MY) are numbered here following the scheme of [14]. Figure 1 includes the aerobraking hiatus period (MY23, L_S=190°–260°), during which time the orbital period was being reduced from 45 to 24 hours and the configuration was more difficult for atmospheric assimilation [11]. Following this, data are available throughout almost three Martian years of 2-hour period, mapping phase orbits **(**MY24, L_S=141° to MY27, L_S=72°).

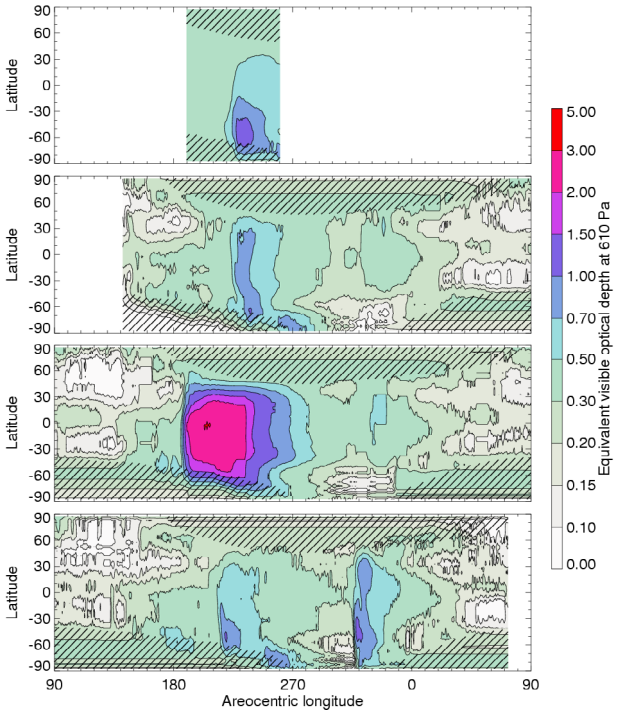

Figure 1: Assimilated dust optical depth at 610 Pa from the full assimilation period. Each panel shows one Martian year, Mars Years 23-26 from upper panel down, with summer solstice at the left-hand edge. The hatched regions indicate where there are few, if any, total dust opacity observations (the mean surface temperature is typically below 160 K).

Transient Waves: The assimilated model analysis can be compared with direct synoptic mapping analyses of TES temperatures [15, 16]. Figure 2 shows an analysis of the zonal wavenumber 1 component of the temperature field on the 30 Pa pressure surface (roughly corresponding to 30 km altitude above the mean surface) at 62.5°N, for direct comparison with Fig. 1(b) of [16]. A very similar pattern of waves is revealed, with evidence of eastward propagating waves present both at a shorter period of about 5–7 days, and with a longer period ranging from about 15–30 days, especially during L_S = 240°–270°, possibly preceded by a strong stationary wave around L_S = 230°.

Figure 3 shows a similar plot for the same period in the following Mars year, MY25. At the start of this plot, the 2001 global dust storm is still underway, and there is some evidence that the waves are of smaller amplitude than at the same time in MY24, consistent with a more stably-stratified atmosphere. Around L_S = 230° onwards, a strong wave becomes increasingly clear, with a period falling from around 5 days at the start of the record to more than 20 days by L_S = 260°, as observed by [16]. This is followed by a re-emergence of the short period wave from L_S = 290°.

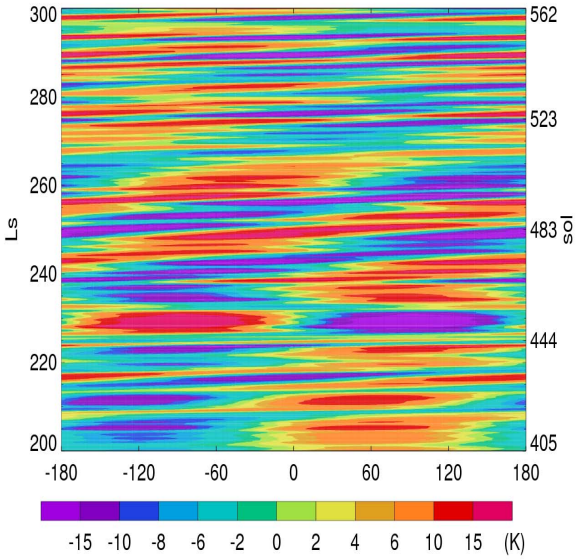

Figure 2: Hovmoller plot showing the non-diurnal component of the zonal wavenumber 1 temperature anomaly on the 30 Pa pressure surface at 62.5°N. The axes are areocentric longitude (L_S) and longitude in degrees East. Model day number (sol) is shown on the right-hand axis, with sol 0 corresponding to spring equinox in MY 24. This plot shows northern hemisphere autumn and winter in MY24.

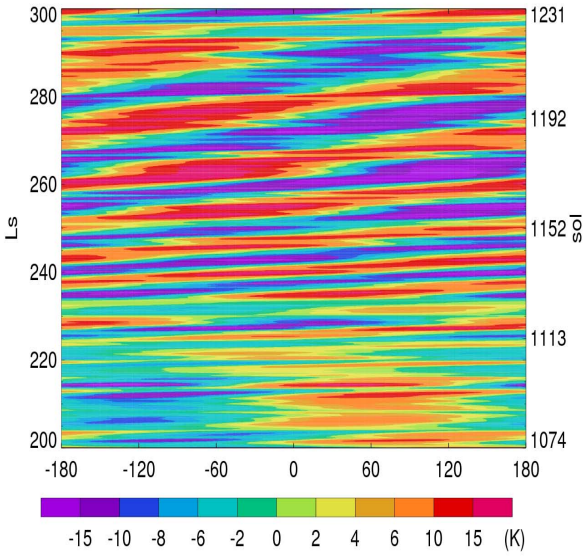

Figure 3: As Fig. 2, but for the same period in northern hemisphere autumn and winter in the following year, MY25. The 2001 global dust storm had begun at L_S = 185° and higher levels of dust persisted throughout the earlier part of this diagram, see Fig. 1.

Figures 4 and 5 summarize the total transient standard deviation in temperature associated with all variance on timescales of longer than one day, i.e. not including the atmospheric thermal tides, as a function of latitude and log(pressure). Figure 3 is for a period just before northern hemisphere winter solstice, when the transient variability in the atmosphere is large, especially at high latitudes where baroclinic transient waves propagate in the region of the westerly jet in the winter hemisphere, as found by [16]. In contrast, Fig. 4 shows a period from later in the winter, just before northern spring equinox. At this time, waves in the northern hemisphere are stronger near the surface than they are around winter solstice, but they are much more strongly trapped at low altitudes and are relatively weak in the middle and upper atmosphere. There is also some evidence of weak transient wave activity near the surface in the southern hemisphere, as it reaches the southern autumn equinox.

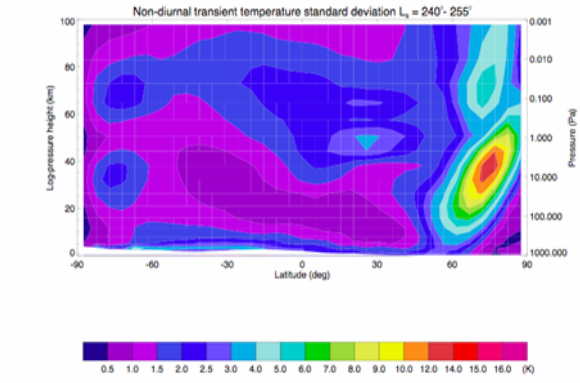

Figure 4: Transient temperature standard deviation (K) at L_S = 240°–255°.

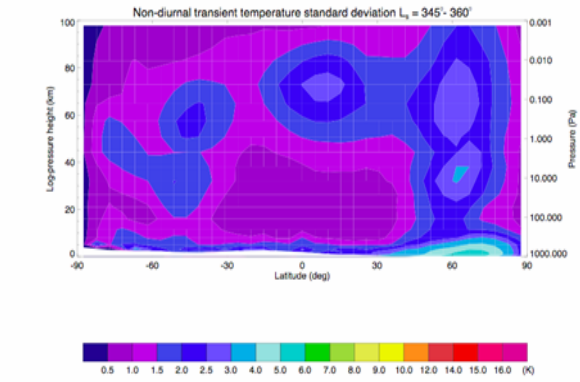

Figure 5: As Fig. 4 at L_S = 345°–360°.

The assimilation permits analysis of other fields than those measured directly. Figure 6 illustrates the longitudinal mean of the root-mean-square meridional wind variability on the 400 Pa pressure surface (roughly 4 km above the mean surface), as a function of latitude and time of year. This clearly shows regions where the transient wave activity is large, notably in the winter hemisphere, but peaking just after autumn equinox and again before spring equinox, with a secondary minimum around winter solstice in each year and hemisphere. There is also transient wave activity in the southern hemisphere, but it is much weaker than that seen in the northern hemisphere. There is evidence of interannual variability in the strength of the transient waves, especially evident in the weaker waves seen around the time of the global dust storm from L_S = 185° onwards in MY25.

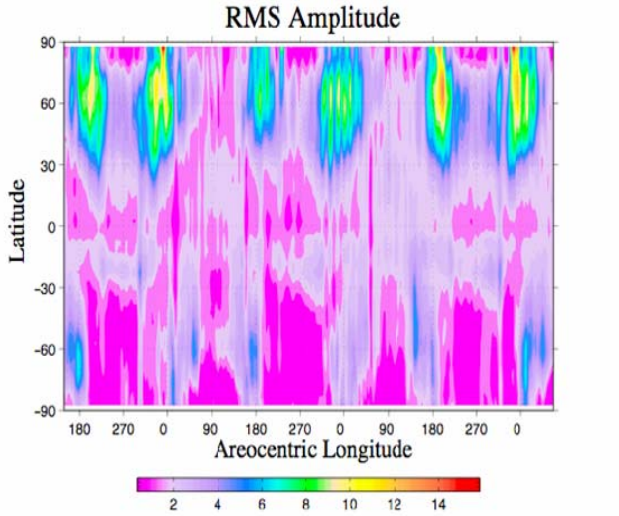

Figure 6: Root-mean-square amplitude of the variability of the meridional velocity (m/s) on the 400 Pa pressure surface as a function of latitude throughout the MY24, L_S=141° to MY27, L_S=72° period.

The regular sampling of the assimilated model data permits a straightforward Fourier analysis in longitude and time to identify zonal wavenumbers and their associated periods; generally longer periods of 5–30 days are associated with the zonal wavenumber 1 wave, whereas zonal wavenumbers 2 and 3 show significant amplitudes at shorter periods of 2–4 days. These three low zonal wavenumber modes tend to dominate all higher wavenumbers in the reanalysis record.

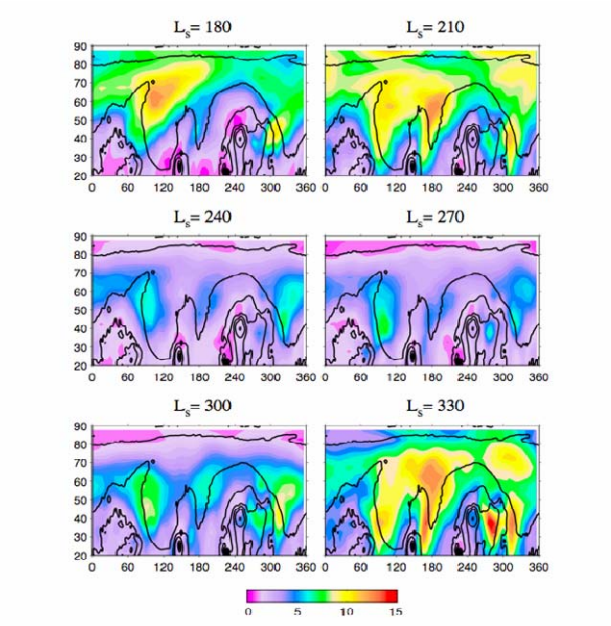

Figure 7: Root-mean-square variability of the meridional velocity (m/s) on the 400 Pa pressure surface in the northern hemisphere shown at intervals throughout the northern hemisphere winter of MY24. The solid contours show the topography for reference. Axes are latitude in degrees North and longitude in degrees East.

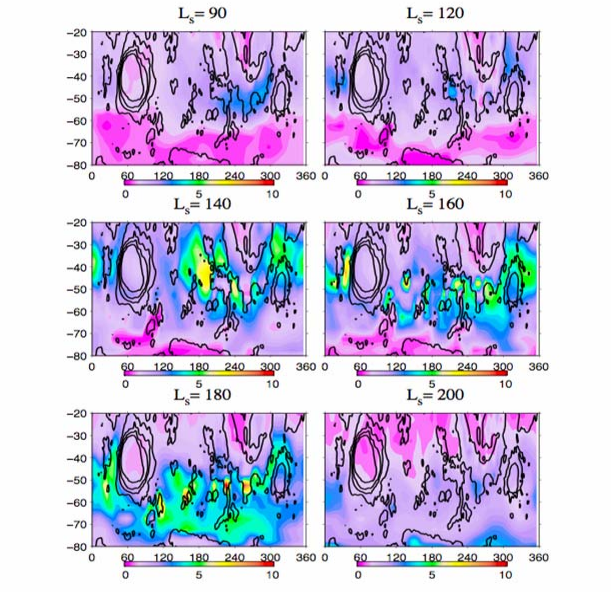

Figure 8: As Fig. 7, but for the southern hemisphere at intervals throughout the southern hemisphere winter of MY26.

Figures 7 and 8 show the presence of mid-latitude 'storm zones' [18]. These are spatial structures associated with the transient wave variability, shown at six intervals throughout northern hemisphere and southern hemisphere winter from the first and third years of the mapping phase assimilation respectively. The strong topographic modulation of the transient waves is clear in each case, with regions of enhanced variability over the lowlands to the east of Tharsis, Syrtis Major and Elysium. In the southern hemisphere, the Hellas basin breaks the symmetry of the weaker storm track, which moves southward as the season progresses and the seasonal polar ice cap retreats,.

Future Plans: The assimilation technique described here has proved robust and reliable for the entire TES/MGS period. Recent developments in data assimilation for the Earth, e.g. 4D-Var and the ensemble Kalman filter, should allow an improved analysis to be conducted, and this is the subject of current study. Data from Mars Climate Sounder on Mars Reconnaissance Orbiter will provide a new opportunity to assimilate an extended atmospheric data set from a single orbiting satellite, a configuration that has already proved successful in the present study.

The results of these assimilations are intended to be accessible to the wider scientific community. This presents a practical challenge, since even the 2-hourly data set from a single, relatively moderate resolution model which has been run for three Mars years is several tens of gigabytes. One option is the production of climate statistics [17], but this results in the loss of detailed information describing transient atmospheric waves, such as those described in the present paper.

References: [1] Conrath B. J. et al. (2000) *JGR, 105 (E4),* 9509–9519. [2] Smith M. D. et al. (2001) *JGR, 106 (E10),* 23929–23945. [3] Smith M. D. et al. (2002) *Icarus, 157 (1),* 259–263. [4] Smith M. D. (2004) *Icarus, 167 (1),* 148–165. [5] Wilson R. J. et al. (2007) *7th International Conference on Mars.* [6] Montabone L. et al. (2007) *7th International Conference on Mars.* [7] Forget F. et al. (1999) *JGR, 104 (E10),* 24155–24176. [8] Lorenc et al. (1991) *Quart. J. Roy. Meteorol. Soc., 117,* 59–89. [9] Lewis S. R. et al. (1996) *Planet. Space Sci., 44,* 1395–1409. [10] Lewis S. R. et al. (1997) *Adv. Space Res., 19,* 1267–1270. [11] Lewis et al. (2007) *Icarus,* submitted. [12] Lewis S. R. and Barker P. (2005) *Adv. Space Res., 36,* 2162–2168. [13] Montabone L. et al. (2006) *Icarus, 185 (1),* 113–132. [14] Clancy R. T. et al. (2000) *JGR, 105 (E4),* 9553–9571. [15] Banfield D. et al. (2003) *Icarus, 161 (2),* 319–345. [16] Banfield D. et al. (2004) *Icarus, 170 (2),* 365–403. [17] Lewis S. R. et al. (1999) *JGR, 104 (E10),* 24177–24194. [18] Hollingsworth J. L. et al. (1996) *Nature, 380,* 413–416.